NJC

PAPER

View Article Online
View Journal

Cite this: DOI: 10.1039/c8nj01006d

Novel phenanthroimidazole-based blue AIEgens: reversible mechanochromism, bipolar transporting properties, and electroluminescence†

Zhong-Yi Wang,[a] Jue-Wen Zhao,[b] Peng Li,[a] Tong Feng,[a] Wen-Jian Wang,[a] Si-Lu Tao *[b] and Qing-Xiao Tong *[a]

Multifunctional materials are crucial and have promising applications in a wide range of organic electronics. Herein, we designed and synthesized two bipolar blue molecules named 2-(4-(4,5-diphenyl-2-(4-(1,2,2-triphenylvinyl)phenyl)-1*H*-imidazol-1-yl)phenyl)-1-phenyl-1*H*-phenanthro[9,10-*d*]imidazole (**PPI-PIM-TPE**) and 1-phenyl-2-(4-(2-(4-(1,2,2-triphenylvinyl)phenyl)-1*H*-phenanthro[9,10-*d*]imidazol-1-yl)phenyl)-1*H*-phenanthro-[9,10-*d*]imidazole (**2PPI-TPE**) with aggregation-induced emission (AIE) and mechanochromism characteristics. They both have good thermal stability (T_d is 505 °C for **PPI-PIM-TPE** and 510 °C for **2PPI-TPE**), strong AIE properties and reversible mechanochromism. The quantum yields in the solid state were as high as 61.9% for **PPI-PIM-TPE** and 73.4% for **2PPI-TPE**. In addition, the two pristine solid powders are white and emit blue light. After grinding, the solid becomes yellow and emits blue-green emission. The color changes are reversible by solvent fuming. The change in emission color can be observed by the naked eye, demonstrating that they are typical mechanochromic materials. Non-doped blue OLEDs based on **2PPI-TPE** exhibit an external quantum efficiency (EQE), current efficiency (CE) and power efficiency (PE) of 2.48%, 6.46 cd A^{-1} and 4.72 lm W^{-1}, respectively. The doped device based on **2PPI-TPE** as a dopant emitter exhibits a higher EQE, CE and PE of 3.55%, 6.67 cd A^{-1} and 5.52 lm W^{-1}. The performances of the OLEDs with these emitters are among the best of recent reports based on blue materials with AIE and mechanochromism simultaneously.

Received 1st March 2018,
Accepted 17th April 2018

DOI: 10.1039/c8nj01006d

rsc.li/njc

Introduction

Blue organic light-emitting devices (OLEDs) have been attracting extensive attention due to their importance in full-color displays and solid lighting.[1] Blue emission is essential because it is not only one of the primary colors, but it can also reduce power consumption efficiently and extend the color gamut.[2] However, highly efficient blue emitters are relatively under-developed because of their contradictory optical and electrical properties.[3] In addition, to achieve commercially viable OLED products with high electroluminescence (EL) efficiency and reliable working stability, robust luminescent materials with excellent solid-state photoluminescence (PL) efficiency are of vital importance. However, most conventional organic chromophores are only emissive in solution, and suffer detrimental aggregation-caused quenching (ACQ) of their fluorescence due to the formation of excimers or exciplexes in the solid state.[4]

Fortunately, since a new type of luminogen was reported by Tang *et al.* in 2001, AIEgens with a propeller-like structure have emerged and become a hot research topic. They usually emit weakly in solution but much more strongly in the aggregated state due to the restricted intramolecular motion (RIM) of some aromatic rings.[5] This has become an important method for achieving highly luminescent solids as this type of compound typically features a twisted molecular structure that can avoid the close packing of luminophores. AIE molecules are highly emissive in the solid state and have been successfully used in OLEDs.[6] AIE-type blue materials can simultaneously realize blue EL emission and high device efficiencies. By adopting an AIE motif in the molecular design, highly efficient solid-state luminescent materials are readily achievable. For instance, just by combining the AIE units with ACQ functional groups at the molecular level, new AIEgens with excellent PL efficiencies are attainable, allowing non-doped OLEDs utilizing them as emitting layers to perform efficiently, with EL efficiencies reaching or even exceeding the theoretical limit.[7]

[a] *Department of Chemistry, Shantou University, No. 243, University Road, Shantou, Guangdong, 515063, P. R. China. E-mail: qxtong@stu.edu.cn*
[b] *School of Optoelectronic Information, University of Electronic Science and Technology of China (UESTC), Chengdu, 610054, P. R. China. E-mail: silutao@uestc.edu.cn*

† Electronic supplementary information (ESI) available: X-ray crystallographic information files. CCDC 1818717 (**2PPI-TPE**). For ESI and crystallographic data in CIF or other electronic format see DOI: 10.1039/c8nj01006d

As is well known, luminescent organic compounds are widely used in OLEDs, bio-sensing, bio-imaging, chemosensors and mechano-sensors.[8] Mechanochromic materials change their color in response to external mechanical stimuli.[9] AIEgens have potential applications in mechanochromism due to their intrinsic structure, but relevant reports combining AIE and mechanochromic properties in one molecule are rare.[10]

In this article, an improved method to overcome ACQ might involve bisimidazole molecular design to obtain high fluorescence quantum yield blue light emission. We exploit the novel strategy of molecular heredity in developing AIEgens with mechanochromic luminophores. Phenanthroimidazole is a nitrogen-containing heterocyclic conjugated group with a rigid planar structure, possessing excellent thermal properties, high fluorescence quantum yield, and bipolar transporting properties, and has attracted tremendous attention as a building block for blue-emitters.[11] However, it possesses a rigid planar structure that leads to typical π–π stacking. The introduction of an AIE unit into phenanthroimidazole derivatives may be a strategy to inhibit this interaction.[12] Here, we introduced the large twist and steric hindrance of tetraphenylethene to inhibit intermolecular aggregation and π–π stacking in the solid state. Here, we designed and synthesized two blue fluorescence materials, **PPI-PIM-TPE** and **2PPI-TPE** (Fig. 1). No typical π–π stacking was observed in the single crystal of **2PPI-TPE**. On the other hand, in the film PL state, **PPI-PIM-TPE** and **2PPI-TPE** show blue emission around 436 nm and 465 nm. The solid quantum yields still remain as high as 61.9% for **PPI-PIM-TPE** and 73.4% for **2PPI-TPE** by the integrating sphere method. Simultaneously, the two materials showed obvious mechanochromic properties. The two pristine solid powders are white and emit blue light at 438 nm for **PPI-PIM-TPE** and 465 nm for **2PPI-TPE**. After grinding, the solid becomes yellow and shows blue-green emission at 450 nm for **PPI-PIM-TPE** and 480 nm for **2PPI-TPE**. The color changes are reversible by solvent fuming. The change in emission color can be observed by the naked eye, demonstrating that they are typical mechanochromic materials. In addition, **PPI-PIM-TPE** and **2PPI-TPE** showed excellent AIE properties.

The two compounds show excellent photophysical properties; they have high thermal stability, the decomposition temperature (T_d) is 505 °C for **PPI-PIM-TPE** and 510 °C for **2PPI-TPE**, and the glass-transition temperature of **PPI-PIM-TPE** is as high as 125 °C. As for the electroluminescence properties of **PPI-PIM-TPE** and **2PPI-TPE**, the maximum CE, PE and EQE are 5.20 cd A^{-1}, 3.39 lm W^{-1} and 2.41% for **PPI-PIM-TPE** and 6.64 cd A^{-1}, 4.72 lm W^{-1} and 2.48% for **2PPI-TPE** for the non-doped devices. The doped device for **2PPI-TPE** also showed high performance, and the EQE_{max} reached 3.55%. These results confirm that this novel design strategy is efficient for tuning the performance of devices and intermolecular aggregation.

Results and discussion

Synthesis and characterization

The synthesis routes of **PPI-PIM-TPE** and **2PPI-TPE** are depicted in Scheme 1. The starting materials **1** and **2** were prepared according to the literature.[13] Finally, a classical "one-pot" reaction was adopted to synthesize the target products **PPI-PIM-TPE** and **2PPI-TPE** in good yields. The compounds were then purified using a silica column and characterized with ^{1}H NMR and ^{13}C NMR spectroscopy, mass spectrometry and elemental analysis.

Thermal properties

The thermal properties of **PPI-PIM-TPE** and **2PPI-TPE** were investigated with thermogravimetric analysis (TGA) and differential scanning calorimetry (DSC) under a nitrogen atmosphere at a heating rate of 10 °C min^{-1}, as shown in Fig. 2. Their decomposition temperatures (T_d, corresponding to 5% weight loss) were measured to be 505 °C and 510 °C for **PPI-PIM-TPE** and **2PPI-TPE**, respectively. Additionally, the glass-transition temperature of **PPI-PIM-TPE** is 125 °C, while no obvious glass transition and an endothermic melting transition could be observed for **2PPI-TPE**. These results suggest that the two molecules possess good thermal and morphological stabilities. The detailed data are summarized in Table 1.

Photophysical properties

Both compounds have good solubility in common organic solvents, such as dichloromethane, chloroform and tetrahydrofuran (THF). Fig. 3a shows their absorption spectra in diluted THF solutions. **PPI-PIM-TPE** and **2PPI-TPE** demonstrate similar absorptions, in which the bands at around 300 and 350 nm can be ascribed to the π–π* transition of the phenanthroimidazole moiety, and the 262 nm absorption band is caused by the π–π* transition of the benzene ring connected to the N atom in the imidazole ring.

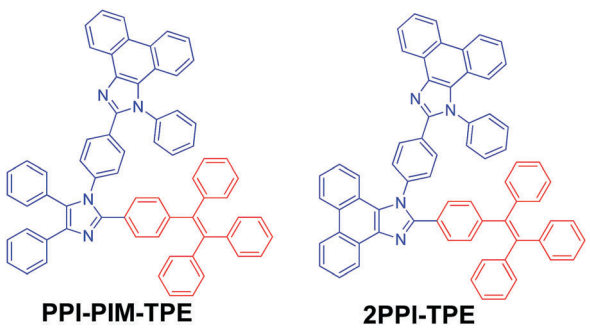

Fig. 1 Molecular structures of **PPI-PIM-TPE** and **2PPI-TPE**.

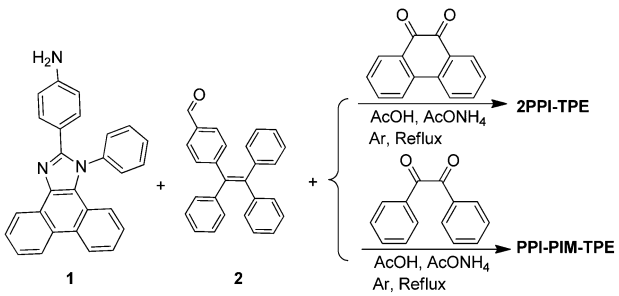

Scheme 1 Synthesis routes of **2PPI-TPE** and **PPI-PIM-TPE**.

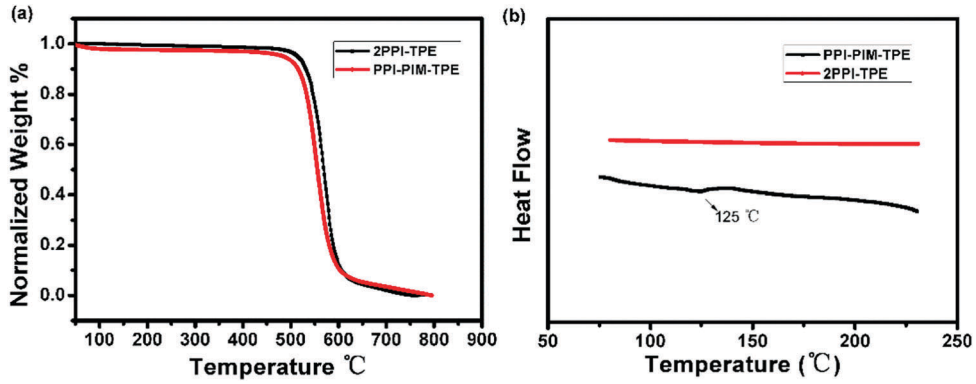

Fig. 2 TGA (a) and DSC (b) curves of **PPI-PIM-TPE** and **2PPI-TPE**.

Table 1 The thermal and photophysical properties of **PPI-PIM-TPE** and **2PPI-TPE**

Compound	T_d[a] [°C]	T_g[b] [°C]	HOMO[c] [eV]	LUMO[d] [eV]	λ_{abs}[e] [nm]	λ_{em}[e] [nm]	λ_{em}[f] [nm]	Φ_f(solid)[g] [%]
PPI-PIM-TPE	505	125	−5.46	−2.37	262, 335, 355	438	460	61.9
2PPI-TPE	510	—	−5.37	−2.38	263, 335, 354	450	460	73.4

[a] 5% weight loss temperature. [b] —, not observed. [c] The energy levels were calculated from the energy level of the ferrocene (Fc) reference (4.80 eV). [d] Detected *via* E_g from the HOMO levels, LUMO = HOMO + E_g. [e] Measured in dilute THF solution (10^{-5} mol L^{-1}). [f] Measured in a film. [g] The solid state quantum yield on the quartz plate using an integrating sphere apparatus.

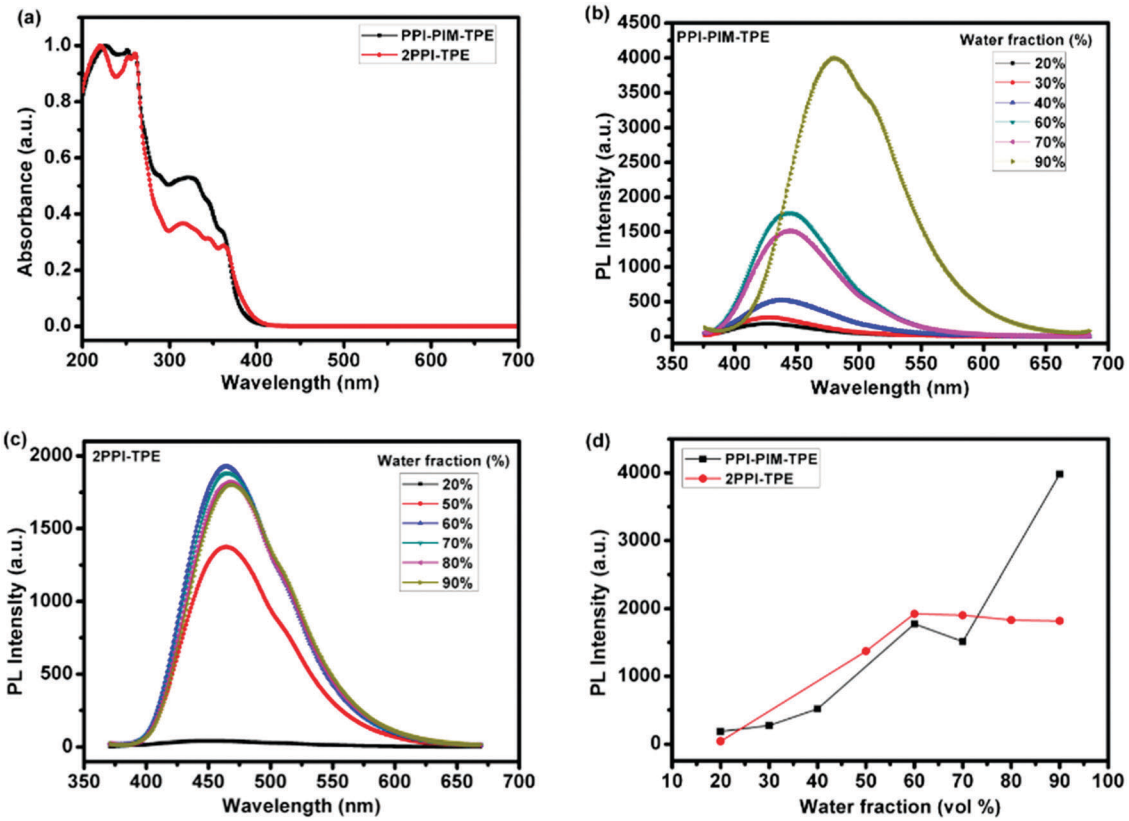

Fig. 3 (a) Electronic absorption spectra of **PPI-PIM-TPE** and **2PPI-TPE** recorded in THF. Fluorescence spectra of (b) **PPI-PIM-TPE** and (c) **2PPI-TPE** in THF/water mixtures with different water fractions. (d) Plot of fluorescence intensity (PL) *vs.* % water fraction (f_w).

Their PL properties were also studied in THF/water mixtures, with different water fractions (f_w), to investigate the effects of aggregation on their emission process. Fig. 4 clearly shows the PL changes and fluorescence images of these new luminogens in

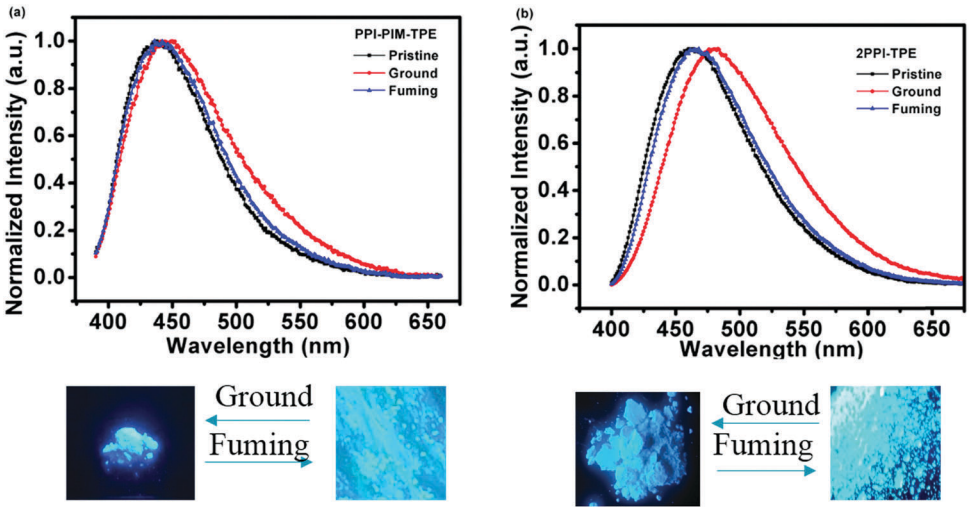

Fig. 4 Emission spectra of **PPI-PIM-TPE** (a) and **2PPI-TPE** (b) as-synthesized, ground and as annealed solids and photographs taken under 354 nm UV illumination.

a THF/water mixture. **PPI-PIM-TPE** and **2PPI-TPE** were nearly non-emissive in pure THF solution, but they became highly fluorescent in higher water fraction mixtures, which reveals that they are AIE active. A different percentage water fraction was required for **PPI-PIM-TPE** and **2PPI-TPE** to initiate the AIE effect. The PL intensity was obviously changed for both compounds when the f_w value was increased from 0 to 60 vol%. However, the emission intensity was drastically increased upon further increase of the water content due to the formation of aggregates. When f_w reached 90 vol% for **PPI-PIM-TPE** and 60 vol% for **2PPI-TPE**, the PL intensity reached the maximum. The experimental results clearly demonstrate that **PPI-PIM-TPE** and **2PPI-TPE** are AIE-type compounds.[14]

Mechanochromism

The mechanical stimuli-responsive properties of **PPI-PIM-TPE** and **2PPI-TPE** were studied using emission spectroscopy. We observed deep-blue emission peaking at 438 nm for the as-prepared solid of **PPI-PIM-TPE**. After grinding, the emission color changed to sky-blue (450 nm). The deep-blue emission was restored by a solvent fuming process, as shown in Fig. 4a. Fig. 4b indicates that **2PPI-TPE** shows good color contrast reversible mechanochromic behavior between sky-blue and yellow-green color. The pristine solid of **2PPI-TPE** shows blue color emission, with an emission maximum at 450 nm. Upon grinding using a mortar and pestle, the blue-emitting pristine solid was converted to a yellowish green emitting solid and the emission peak was red-shifted to 480 nm. Simultaneously, the absolute Φ_f of **PPI-PIM-TPE** and **2PPI-TPE** was reduced from 61.9% to 53.8% and 73.4% to 69.8% by grinding the as-prepared solids into an amorphous state. The relevant data are summarized in Table 2.

The powder XRD study of the pristine, ground and fumed forms of **PPI-PIM-TPE** and **2PPI-TPE** were performed to understand the mechanochromic properties as shown in Fig. 5. The as-prepared solids showed much more and sharper diffraction, indicating their crystalline properties. However, the signals of the ground solids are rather weak, evidencing the disordered molecular packing. The fumed samples show some sharp diffractions again after solvent fuming, revealing the restoration of the crystalline lattice. These results clearly suggest a change in the molecular arrangement due to grinding.

Table 2 Summary of the mechanochromic properties of **PPI-PIM-TPE** and **2PPI-TPE**

Compound	$\lambda_{em}{}^a$ [nm]	Φ_f(solid)^a [%]
PPI-PIM-TPE	438/450/441	73.4/69.8/66.8
2PPI-TPE	450/480/458	61.9/53.8/49.4

[a] Measured at room temperature for the pristine, ground, and fumed powders.

Single crystal structures

The single crystal X-ray structure of **2PPI-TPE** provides an insight into its AIE. Usually, phenanthroimidazole unit-containing fluorophores are known to have planar structures and extensive π···π staking interactions, but the crystal structure of **2PPI-TPE** exhibits a twisted conformation suppressing the π···π staking effect of the phenanthroimidazole and supporting its AIE active nature. Furthermore, the twisting in the phenyl rings supports the intramolecular rotations in solution leading to poor fluorescence.[15] The single crystal structure of **2PPI-TPE** displays the modes of intermolecular interactions in its crystal, including N···H–C (2.968 Å) and C–H···π (2.322 Å) interactions. In addition, two adjacent molecules were packed *via* excellent weak π–π interactions (5.136 Å). These multiple interactions (N···H–C (2.968 Å) and C–H···π (2.322 Å)) should be mutable to external forces. When the crystalline lattice collapses in response to external stimuli, the emitters may adjust to a more planar conformation, leading to red-shifted emission.[16] In Fig. 6c, the molecular packing of **2PPI-TPE**

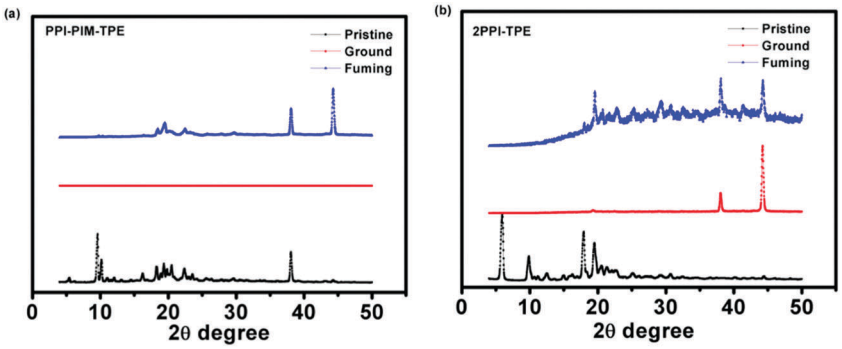

Fig. 5 PXRD curves of **PPI-PIM-TPE** (a) and **2PPI-TPE** (b) in their as-synthesized, ground and annealed forms.

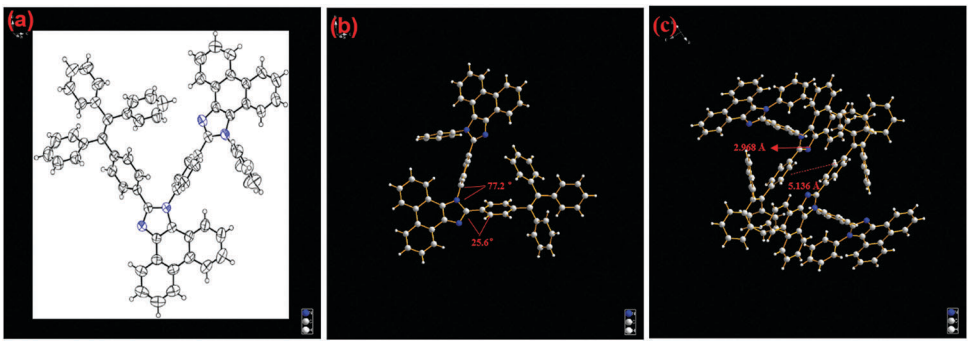

Fig. 6 Molecular ORTEP structure (a), single crystal structure (b) and molecular packing (c) of **2PPI-TPE**.

reveals that the PPI and TPE moieties separately aggregate into stacked columns, indicating that the electron and hole transport channels, respectively, are perfectly constructed.

Theoretical calculations

To further explore the structure–property relationship, we carried out Density Functional Theory (DFT) calculations (B3lyp/6-31g*) to obtain the optimized structures and orbital distributions of the LUMO and HOMO energy levels of **PPI-PIM-TPE** and **2PPI-TPE**, as shown in Fig. 7. The HOMO of **PPI-PIM-TPE** is predominantly located on the phenylimidazole and TPE units, while the LUMO is distributed on the phenanthroimidazole and TPE units. Overall, the molecular orbital distribution of **2PPI-TPE** is similar to that of **PPI-PIM-TPE**. This is more likely to endow them with a bipolar charge transporting ability and more efficient luminescence as the emitter in an OLED.[17]

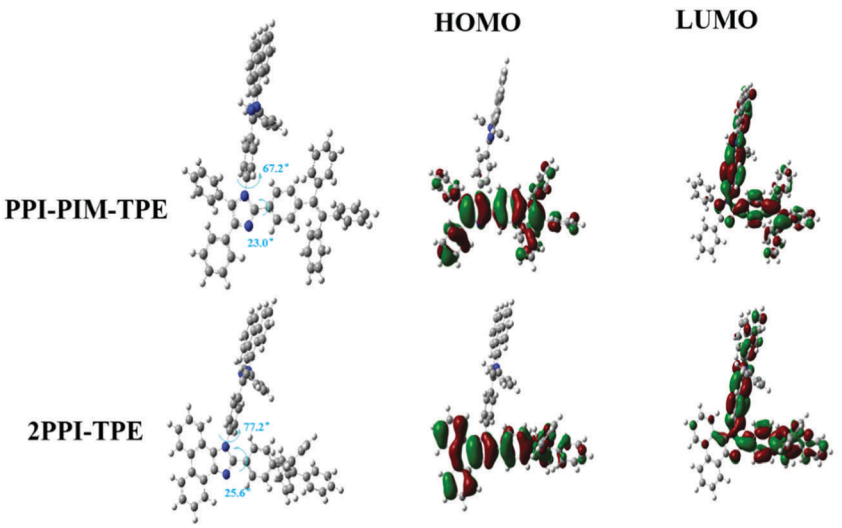

Fig. 7 Optimized structure and spatial distribution of the HOMO and LUMO of **PPI-PIM-TPE** and **2PPI-TPE**.

Electrochemical properties

Cyclic voltammetry (CV) was performed to investigate the electrochemical properties of the molecules. As shown in Fig. S1 (ESI†), the HOMO levels were measured to be −5.46 and −5.37 eV for **PPI-PIM-TPE** and **2PPI-TPE**, from the onset of the oxidation curves, referring to the equation: HOMO = $-(4.80 + E_{ox})$ eV.[18] The LUMO levels were estimated from the HOMO levels and the energy gaps (E_g) determined from the onset of the absorption spectra. Therefore, the LUMO levels were further projected to be −2.37 and −2.38 eV for **PPI-PIM-TPE** and **2PPI-TPE**. These values are lower than that of phenanthroimidazole (−2.16 eV). Clearly, the electron injection ability of **PPI-PIM-TPE** and **2PPI-TPE** is similar to that of 1,3,5-tri(phenyl-2-benzimidazolyl)-benzene (TPBi, −2.7 eV), but better than that of phenanthroimidazole.[19] This suggests a good carrier injection property in **PPI-PIM-TPE** and **2PPI-TPE**, due to their suitable HOMO and LUMO energy levels. This property allowed the fabrication of devices with simple configurations, which is an advantage for practical OLED applications.[20]

Single carrier devices

To investigate the charge transport characteristics of the two compounds, we fabricated hole- and electron-only devices with the configurations of indium tin oxide (ITO)/NPB (10 nm)/**PPI-PIM-TPE** or **2PPI-TPE** (100 nm)/NPB (10 nm)/Al (100 nm) for the hole-only device and ITO/TPBI (10 nm)/**PPI-PIM-TPE** or

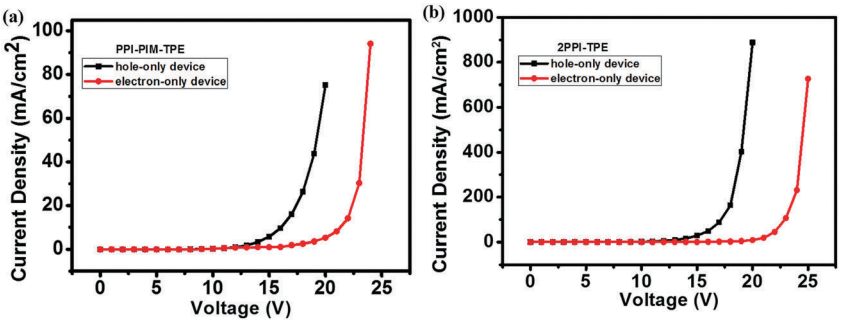

Fig. 8 Current density *versus* voltage characteristics of the hole-only and electron-only devices for **PPI-PIM-TPE** (a) and **2PPI-TPE** (b).

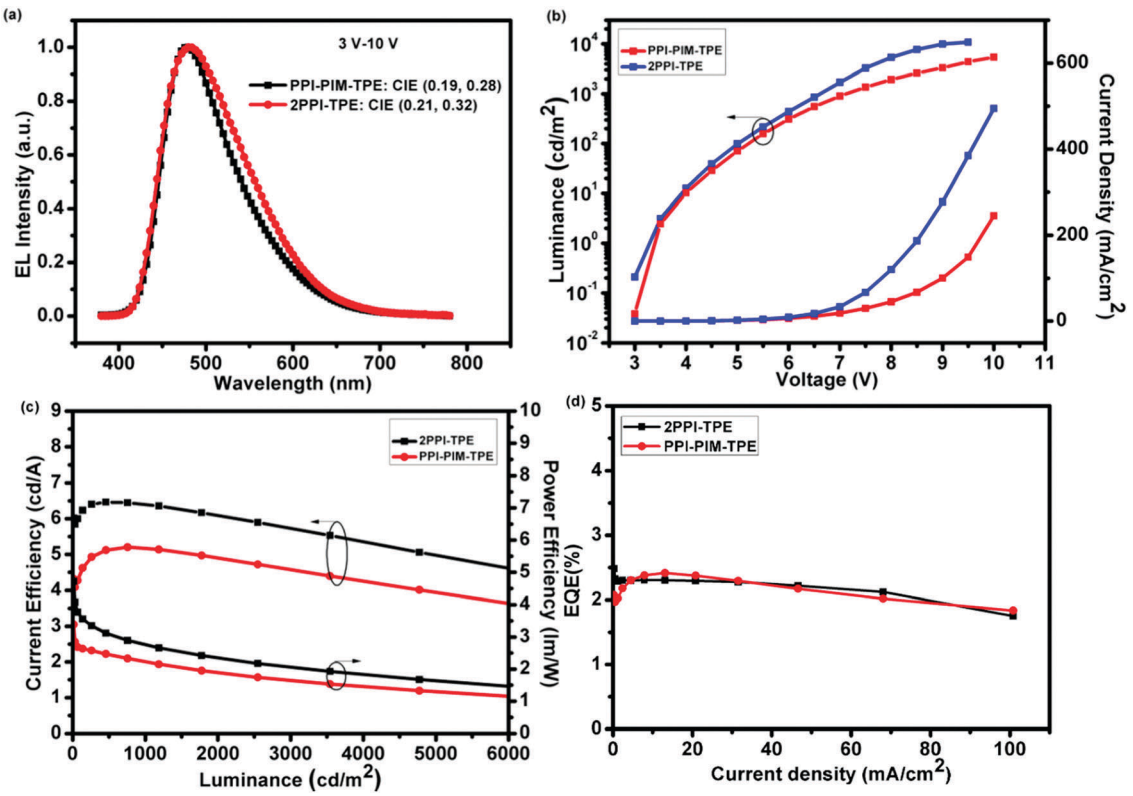

Fig. 9 (a) EL spectra and the corresponding CIE coordinates at different voltages, (b) current density–voltage–luminescence characteristics, (c) plots of CE and PE *versus* luminance, and (d) EQE *versus* current density plots of the non-doped light-emitting devices based on **PPI-PIM-TPE** and **2PPI-TPE**.

2PPI-TPE (100 nm)/TPBi (10 nm)/LiF (1 nm)/Al (100 nm) for the electron-only device. As shown in Fig. 8, it is obvious that both devices can conduct significant current, indicating the bipolar transporting abilities of both **PPI-PIM-TPE** and **2PPI-TPE**.[21] Therefore, balancing the carrier transporting properties will be expected to reveal why the devices based on **PPI-PIM-TPE** and **2PPI-TPE** achieved relatively lower turn-on voltages and higher current density luminescence, which are important factors for the device efficiencies.[22]

Electroluminescence properties

The efficient solid-state blue emission of **PPI-PIM-TPE** and **2PPI-TPE**, as well as their high thermal stability and suitable HOMO and LUMO levels, prompted us to investigate their EL properties. We fabricated non-doped OLED devices with a simple configuration of ITO/NPB (65 nm)/**PPI-PIM-TPE** or **2PPI-TPE** (20 nm)/TPBi (35 nm)/LiF (1 nm)/Al (100 nm). In this device, **PPI-PIM-TPE** and **2PPI-TPE** function as a blue emitting layer (EML). *N*,*N*′-Bis-(1-naphthyl)-*N*,*N*′-diphenyl-1,10-biphenyl-4,4′-diamine (NPB) functions as a hole-transporting layer, and 1,3,5-tri(phenyl-2-benzimidazolyl)-benzene (TPBi) serves as an electron-transporting layer. The EL spectrum peaked at 476 nm for the **PPI-PIM-TPE** device and 480 nm for the **2PPI-TPE** device, and the CIE coordinates were (0.19, 0.28) for **PPI-PIM-TPE** and (0.21, 0.32) for **2PPI-TPE**. No new peaks are observed under different operation voltages (Fig. S2, ESI†), indicating that carrier recombination is well confined within the EML.[23] Fig. 9b shows the current density–voltage–luminescence (*J*–*V*–*L*) curves, which indicate that both devices have very low turn-on voltages (3 V for **PPI-PIM-TPE** and **2PPI-TPE**), revealing the small energy gap in the devices. As shown in Fig. 9c and d, the **PPI-PIM-TPE**-based non-doped device showed a maximum external quantum efficiency (EQE), current efficiency (CE) and power

Table 3 The performance of the devices based on **PPI-PIM-TPE** and **2PPI-TPE**

Emitter	V_{on} [a] [V]	λ_{EL} [nm]	CE_{max} [b] [cd A^{-1}]	PE_{max} [c] [lm W^{-1}]	EQE_{max} [d] [%]	L_{max} [cd m^{-2} V]	CIE [*x*, *y*]
A	3.0	476	5.20	3.39	2.41	5399	(0.19, 0.28)
B	3.0	480	6.46	4.72	2.48	10 830	(0.21, 0.32)
C	3.5	465	5.36	3.37	2.97	8604	(0.17, 0.22)
D	3.5	465	6.67	5.52	3.55	12 930	(0.17, 0.22)

Devices structure: A and B: ITO/NPB (65 nm)/**PPI-PIM-TPE** or **2PPI-TPE** (20 nm)/TPBi (35 nm)/LiF (1 nm)/Al (100 nm); C and D: ITO/NPB (65 nm)/CPB:**PPI-PIM-TPE** or **2PPI-TPE** (30% by wt, 20 nm)/TPBI (35 nm)/LiF (1 nm)/Al (100 nm). [a] V_{on} is the voltage at 1 cd m^{-2}. [b] The maximum current efficiency. [c] The maximum power efficiency. [d] The maximum external quantum efficiency.

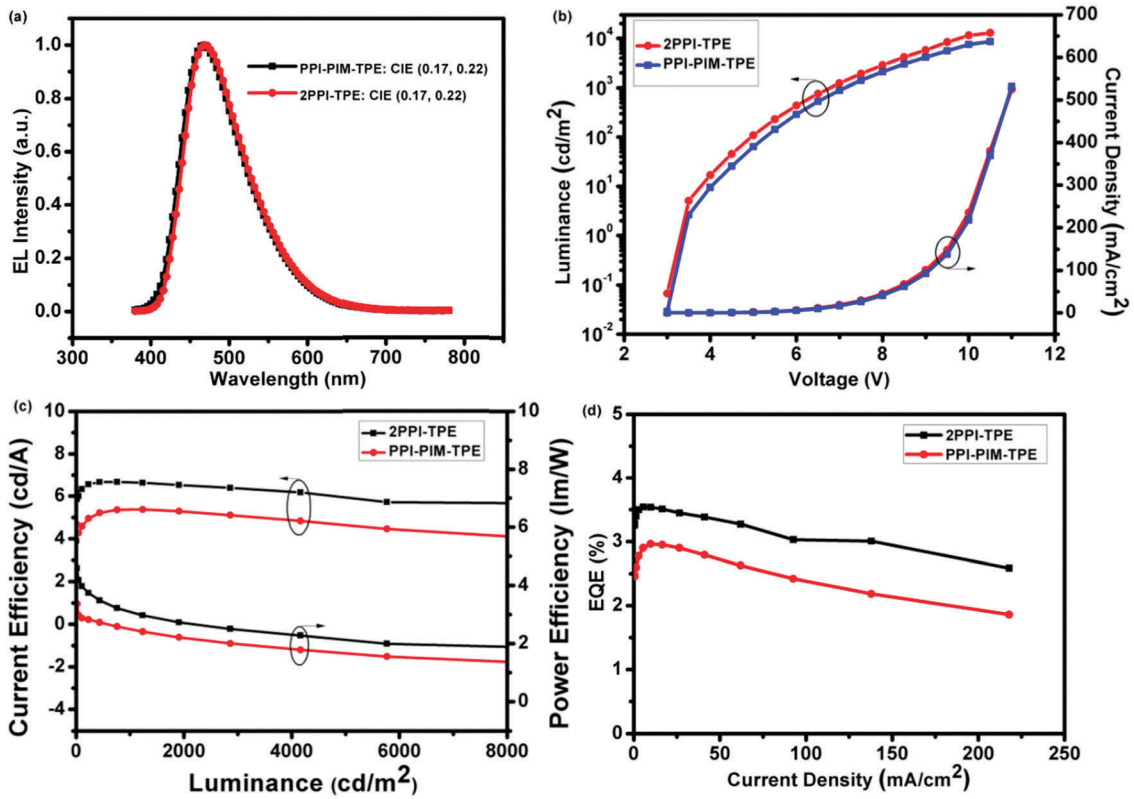

Fig. 10 (a) EL spectra and the corresponding CIE coordinates at different voltages, (b) current density–voltage–luminescence characteristics, (c) plots of CE and PE *versus* luminance, and (d) EQE *versus* current density plots of the non-doped light-emitting devices based on **PPI-PIM-TPE** and **2PPI-TPE**.

efficiency (PE) of 2.41%, 5.20 cd A^{-1} and 3.39 lm W^{-1}, respectively. The **2PPI-TPE** non-doped device also exhibited good performance, exhibiting a maximum EQE, CE and PE of 2.48%, 6.46 cd A^{-1} and 4.72 lm W^{-1}, respectively. The key data of the devices are summarized in Table 3.

To further improve the color purity and device efficiency, the doped OLEDs were constructed with a multilayer structure: ITO/NPB (65 nm)/CPB:**PPI-PIM-TPE** or **2PPI-TPE** (30% wt 20 nm)/TPBI (35 nm)/LiF (1 nm)/Al (100 nm). Here, CPB was selected as the host. The **PPI-PIM-TPE**- and **2PPI-TPE**-doped devices revealed blue emission peaks of 465 nm and CIE coordinates of (0.17, 0.22). The turn-on voltages of the two devices were only 3.5 V. The **PPI-PIM-TPE**-based doped device exhibited a maximum EQE, CE and PE of 2.97%, 5.36 cd A^{-1} and 3.37 lm W^{-1}, respectively. In particular, the device using **2PPI-TPE** as a sky-blue emitter exhibited impressive performance, with a maximum EQE, CE and PE of 3.55%, 6.67 cd A^{-1} and 5.52 lm W^{-1}, respectively. To the best of our knowledge, the performances of the OLEDs with these emitters are among the best of recent reports based on blue materials with AIE and mechanochromism simultaneously.[24] The device characteristics are shown in Fig. 10 and Table 3.

Conclusions

In summary, two new efficient bipolar blue materials, **PPI-PIM-TPE** and **2PPI-TPE**, with AIE and mechanochromic properties were designed and synthesized. The emitters showed reversible high contrast tunable emission in response to external stimuli. Moreover, with AIE characteristics and good thermal stabilities, **PPI-PIM-TPE** and **2PPI-TPE** are suitable for application in OLEDs. The non-doped device based on **PPI-PIM-TPE** exhibits a maximum EQE, CE and PE of 2.41%, 5.20 cd A^{-1} and 3.39 lm W^{-1}, respectively. The doped **PPI-PIM-TPE** device shows a maximum PE, CE and EQE of 3.37 lm W^{-1}, 5.36 cd A^{-1} and 2.97%, respectively. The non-doped EL device fabricated from **2PPI-TPE** shows a low turn-on voltage and maximum EQE, CE and PE of 2.48%, 6.46 cd A^{-1} and 4.72 lm W^{-1}, respectively. In particular, the **2PPI-TPE**-based doped device achieves a maximum EQE, CE and PE of 3.55%, 6.67 cd A^{-1} and 5.52 lm W^{-1}, respectively. Here, we successfully provide a molecular design strategy for high-efficiency blue organic fluorescence materials.

Conflicts of interest

There are no conflicts to declare.

Acknowledgements

This research was supported by the National Natural Science Foundation of China (Project No. 51673113). S. L. Tao would like to thank the National Natural Science Foundation of China (NSFC Grant 51373029, 61421002, 51533005), the Preeminent Youth Fund of Sichuan Province (2015JQ0006) and The Fundamental Research Funds for the Central Universities (ZYGX2015J048) for financial support.

Notes and references

1 C. J. Zheng, J. Wang, J. Ye, M. F. Lo, X. K. Liu, M. K. Fung, X. H. Zhang and C. S. Lee, *Adv. Mater.*, 2013, **25**, 2205.
2 H. Sasabe and J. Kido, *J. Mater. Chem. C*, 2013, **1**, 1699.
3 G. M. Farinola and R. Ragni, *Chem. Soc. Rev.*, 2011, **40**, 3467.
4 (*a*) U. Lemmer, S. Heun, R. F. Mahrt, U. Scherf, M. Hopmeier, U. Siegner, E. O. Gobel, K. Mullen and H. Bassler, *Chem. Phys. Lett.*, 1995, **240**, 373; (*b*) R. Jakubiak, C. J. Collison, W. C. Wan and L. J. Rothberg, *J. Phys. Chem. A*, 1999, **103**, 2394; (*c*) L. Chen, G. Lin, H. Peng, S. Dong, W. Luo, R. R. Hu, S. M. Chen, F. Huang, A. J. Qin, Z. J. Zhao and B. Z. Tang, *Mater. Chem. Front.*, 2017, **1**, 176.
5 (*a*) J. Luo, Z. Xie, J. W. Y. Lam, L. Cheng, H. Chen, C. Qiu, H. S. Kwok, X. Zhan, Y. Liu, D. Zhu and B. Z. Tang, *Chem. Commun.*, 2001, 1740; (*b*) L. Yao, S. Zhang, R. Wang, W. Li, F. Shen, B. Yang and Y. G. Ma, *Angew. Chem.*, 2014, **126**, 2151; (*c*) Q. Li and Z. Li, *Sci. China: Chem.*, 2015, **58**, 1800; (*d*) X. F. Ji, P. Wang, H. Wang and F. H. Huang, *Chin. J. Polym. Sci.*, 2015, **33**, 890; (*e*) J. Mei, N. L. C. Leung, R. T. K. Kwok, J. W. Y. Lam and B. Z. Tang, *Chem. Rev.*, 2015, **115**, 11718.
6 X. Zhan, Z. Wu, Y. Lin, Y. Xie, Q. Peng, Q. Li, D. Ma and Z. Li, *Chem. Sci.*, 2016, **7**, 4355.
7 J. Yang, J. Huang, Q. Li and Z. Li, *J. Mater. Chem. C*, 2016, **4**, 2663.
8 Z. Chi, X. Zhang, B. Xu, X. Zhou, C. Ma, Y. Zhang, S. Liu and J. Xu, *Chem. Soc. Rev.*, 2012, **41**, 3878.
9 (*a*) X. Luo, J. Li, C. Li, L. Heng, Y. Q. Dong, Z. Liu, Z. Bo and B. Z. Tang, *Adv. Mater.*, 2011, **23**, 3261; (*b*) L. Wang, K. Wang, B. Zou, K. Ye, H. Zhang and Y. Wang, *Adv. Mater.*, 2015, **27**, 2918.
10 H. Sun, S. Liu, W. Lin, K. Y. Zhang, W. Lv, X. Huang, F. Huo, H. Yang, G. Jenkins, Q. Zhao and W. Huang, *Nat. Commun.*, 2014, **5**, 3601.
11 (*a*) Y. Dong, B. Xu, J. Zhang, X. Tan, L. Wang, J. Chen, H. Lv, S. Wen, B. Li, L. Ye, B. Zou and W. Tian, *Angew. Chem.*, 2012, **51**, 10782; (*b*) Z. Mao, Z. Yang, Y. Mu, Y. Zhang, Y. F. Wang, Z. Chi, C. C. Lo, S. Liu, A. Lien and J. Xu, *Angew. Chem.*, 2015, **54**, 6270.
12 (*a*) A. Ekbote, S. H. Han, T. Jadhav, S. Mobin, J. Y. Lee and R. Misra, *J. Mater. Chem. C*, 2018, **6**, 2077; (*b*) T. Jadhav, B. Dhokale, S. Mobin and R. Misra, *Chem. Commun.*, 2014, **50**, 9076; (*c*) A. Ekbote, T. Jadhav and R. Misra, *New J. Chem.*, 2017, **41**, 9346.
13 (*a*) T. Jadhav, J. M. Choi, J. Shinde, J. Y. Lee and R. Misra, *J. Mater. Chem. C*, 2017, **5**, 6014; (*b*) X. Zhan, N. Sun, Z. Wu, J. Tu, L. Yuan, X. Tang, Y. Xie, Q. Peng, Y. Dong, Q. Li, D. Ma and Z. Li, *Chem. Mater.*, 2015, **27**, 1847.
14 (*a*) W. Qin, Z. Yang, Y. Jiang, J. W. Y. Lam, G. Liang, H. S. Kwok and B. Z. Tang, *Chem. Mater.*, 2015, **27**, 3892; (*b*) C. Li, S. Wang, W. Chen, J. Wei, G. Yang, K. Ye, Y. Liu and

Y. Wang, *Chem. Commun.*, 2015, **51**, 10632; (*c*) M. T. Lee, C. H. Liao, C. H. Tsai and C. H. Chen, *Adv. Mater.*, 2005, **17**, 2493; (*d*) L. Chen, Y. Jiang, H. Nie, P. Lu, H. H. Y. Sung, I. D. Williams, H. S. Kwok, F. Huang, A. Qin, Z. Zhao and B. Z. Tang, *Adv. Funct. Mater.*, 2014, **24**, 3621.

15 (*a*) G. F. Zhang, H. Wang, M. P. Aldred, T. Chen, Z. Q. Chen, X. Meng and M. Q. Zhu, *Chem. Mater.*, 2014, **26**, 4433; (*b*) G. Zhong, J. B. Sun, P. C. Xue, Z. Q. Zhong, P. Gong, J. Peng and R. Lu, *J. Mater. Chem. C*, 2015, **3**, 2925.

16 (*a*) G. Li, J. Zhao, D. Zhang, Z. Shi, Z. Zhu, H. Song, J. Zhu, S. Tao, F. Lu and Q. X. Tong, *J. Mater. Chem. C*, 2016, **4**, 8787; (*b*) Y. Ooyama and Y. Harima, *J. Mater. Chem. C*, 2011, **21**, 8372; (*c*) Y. Y. Gong, G. Chen, Q. Peng, W. Z. Yuan, Y. Xie, S. Li, Y. M. Zhong and B. Z. Tang, *Adv. Mater.*, 2015, **27**, 6195.

17 T. Jadhav, B. Dhokale, S. M. Mobin and R. Misra, *J. Mater. Chem. C*, 2015, **3**, 9981.

18 W. C. Chen, Q. X. Tong and C. S. Lee, *Adv. Mater.*, 2015, **7**, 2193.

19 (*a*) Z. Wang, P. Lu, S. Chen, Z. Gao, F. Shen, W. Zhang, Y. Xu, H. S. Kwok and Y. Ma, *J. Mater. Chem.*, 2011, **21**, 5451; (*b*) Z. Yang, Z. Chi, T. Yu, X. Zhang, M. Chen, B. Xu, S. Liu, Y. Zhang and J. Xu, *J. Mater. Chem.*, 2009, **19**, 5541; (*c*) Z. L. Zhu, W. C. Chen, L. D. Zhang, X. L. Liu, Q. X. Tong, F. L. Wong, F. Lu and C. S. Lee, *J. Mater. Chem. C*, 2016, **4**, 6249.

20 X. Tang, Q. Bai, Q. Peng, Y. Gao, J. Li, Y. Liu, L. Yao, P. Lu, B. Yang and Y. Ma, *Chem. Mater.*, 2015, **27**, 7050.

21 (*a*) Y. Zhang, T. W. Ng, F. Lu, Q. X. Tong, S. L. Lai, M. Y. Chan, H. L. Kwong and C. S. Lee, *Dyes Pigm.*, 2013, **98**, 190; (*b*) D. He, Y. Yuan, B. Liu, D. Y. Huang, C. Y. Luo, F. Lu, Q. X. Tong and C. S. Lee, *Dyes Pigm.*, 2017, **136**, 347; (*c*) Y. J. Pu, G. Nakata, F. Satoh, H. Sasabe, D. Yokoyama and J. Kido, *Adv. Mater.*, 2012, **24**, 1765.

22 (*a*) N. Chopra, J. Lee, Y. Zheng, S. H. Eom, J. Xue and F. So, *ACS Appl. Mater. Interfaces*, 2009, **1**, 1169; (*b*) Z. L. Zhu, S. F. Ni, W. C. Chen, Y. Yuan, Q. X. Tong, F. L. Wong, F. Lu and C. S. Lee, *Dyes Pigm.*, 2017, **146**, 219; (*c*) X. Tang, L. Yao, H. Liu, F. Shen, S. Zhang, H. Zhang, P. Lu and Y. Ma, *Chem. – Eur. J.*, 2014, **20**, 2149.

23 (*a*) D. Fan, Y. Yi, Z. Li, W. Liu, Q. Peng and Z. Shuai, *J. Phys. Chem. A*, 2014, **119**, 5233; (*b*) X. Han, Q. Bai, L. Yao, H. Liu, Y. Gao, J. Li, L. Liu, Y. Liu, X. Li, P. Lu and B. Yang, *Adv. Funct. Mater.*, 2015, **25**, 7521.

24 (*a*) X. Zhan, Z. Wu, Y. Lin, Y. Xie, Q. Peng, Q. Li, D. Ma. and Z. Li, *Chem. Sci.*, 2016, **7**, 4355; (*b*) Y. Wang, Y. Liao, C. P. Cabry, D. Zhou, G. H. Xie, Z. Qu, D. W. Bruce and W. G. Zhu, *J. Mater. Chem. C*, 2017, **5**, 3999; (*c*) J. Yang, Q. Guo, X. Wen, X. Gao, Q. Peng, Q. Li, D. Ma. and Z. Li, *J. Mater. Chem. C*, 2016, **4**, 8506; (*d*) H. P. Shi, D. H. Xin, X. Gu, P. Zhang, H. Peng, S. Chen, G. Lin, Z. Zhao and B. Z. Tang, *J. Mater. Chem. C*, 2016, **4**, 1228.